Zhang *et al. Miner Miner Mater* 2023;2:3
DOI: 10.20517/mmm.2022.10

Minerals and Mineral Materials

Research Article

Open Access

Differential removal of tetracycline hydrochloride and quinolone antibiotics by calcined and uncalcined layered double hydroxides

Cui Zhang[1,2], J. Viridiana García-Meza[2,3], Yinta Li[1,4,5]

[1]Hubei Key Laboratory of Mineral Resources Processing and Environment, Luoshi Road 122, Wuhan 430070, Hubei, China.
[2]Doctorado Institucional de Ingeniería y Ciencia de Materiales, Universidad Autónoma de San Luis Potosí (UASLP), Sierra Leona 530, San Luis Potosí 78210, Mexico.
[3]Geomicrobiology, Metallurgy Institue, UASLP, Sierra Leona 550, San Luis Potosí 78210, Mexico.
[4]School of Materials Science and Engineering, Weihai Marine Vocational College, Weihai 264200, Shandong, China.
[5]Weihai Key Laboratory of Medical Conditioning Functional Food Processing Technology, Weihai Marine Vocational College, Weihai 264200, Shandong, China.

Correspondence to: Prof./Dr. Yinta Li, School of Materials Science and Engineering, Weihai Marine Vocational College, Haiwan South Road 1000, Weihai 264200, Shandong, China. E-mail: liyinta123@163.com

How to cite this article: Zhang C, García-Meza JV, Li Y. Differential removal of tetracycline hydrochloride and quinolone antibiotics by calcined and uncalcined layered double hydroxides. *Miner Miner Mater* 2023;2:3. https://dx.doi.org/10.20517/mmm.2022.10

Received: 29 Nov 2022 **Revised:** 27 Feb 2023 **Accepted:** 13 Mar 2023 **Published:** 22 Mar 2023

Academic Editor: Feifei Jia **Copy Editor:** Ke-Cui Yang **Production Editor:** Ke-Cui Yang

Abstract

Antibiotics generally cause drug-resistant genes (ARGs) and drug-resistant bacteria (ARBs). With a complex class of antibiotics, it is very crucial to select specific adsorbents for different kinds of antibiotics. Zn-Al layered double hydroxide (LDH) and calcined layered double hydroxide (LDO) were prepared as absorbents for tetracycline hydrochloride (TCH) and ofloxacin (OFX), which were two antibiotics with different structures. According to the results of the adsorption experiments, LDO has the best adsorption capacity on TCH, reaching 322.58 mg/g. Acid-base titration, XRD, TEM, SEM, BET, and FI-TR analyses indicate that LDO has more active sites on the surface, the "memory effect", and a larger specific surface area. In contrast, the removal rate of OFX by LDO is low because OFX has a more stable quinolone ring structure. Furthermore, after five adsorption-desorption cycles, the adsorption rate of TCH remains at 94.9%, demonstrating that LDO has good cyclic adsorption capacity for TCH. This study creatively combines acid-base buffering characteristics to study the mechanism of the adsorption of antibiotics by hydrotalcite, and proposes that LDO can be used as a special adsorbent for TCH.

Keywords: Clay mineral, wastewater treatment, layered double hydroxides, tetracycline hydrochloride, acid-base buffering characteristics

INTRODUCTION

More and more antibiotics are found in natural water bodies, and they always lead to an increase in drug-resistant genes (ARGs) and drug-resistant bacteria (ARB), which result in long-term persistent ecological toxicity[1]. According to survey data, in 2019, residual antibiotics caused more than 2.8 million infections and 35,000 fatalities in the United States[2]. Membrane separation[3], photocatalytic degradation[4], adsorption[5], electrochemical oxidation[6] and others are widely used for antibiotic wastewater treatment. Adsorption with low-cost adsorbents is considered to be the most suitable method[5]. Hu *et al.*[7] concluded that magnetic conjugated microporous polymer hollow spheres (CMP-HSs@Fe_3O_4) potentially adsorb antibiotic molecules effectively. However, not every kind of adsorbent is suitable for antibiotics including quinolones, aminoglycosides, macrolides, oxazolidinones, tetracyclines, etc. Therefore, it is particularly important to use specific adsorbents for various antibiotic wastewater.

Hydrotalcite-type clays belong to a member of layered structure clays, which are also known as layered double hydroxides. It was first discovered in schist deposits in 1,842 by Hochstetter[8], and its catalytic action on hydrogen addition attracted the attention of researchers. Nowadays, various types of layered double hydroxides (LDHs) have been synthesized, and their chemical formula is generally $[M^{II}_{1-X}{}^{2+}M^{III}_{X}{}^{3+}(OH)_2]^{X+}[A_{X/n}]^{n-}.mH_2O$[9]. LDH is a two-dimensional, layered material that can be divided into lamellar cations and interlamellar anions. The interlamellar anions neutralize the positive charges in the main layer, contributing to the electrical neutrality of LDH[10]. The good properties of LDH, including adjustability, alkalinity, thermal stability, and memory effect, result from its unique lamellar structure, which also provides it with an excellent adsorption capacity[11]. Mg-Al-CO_3 LDH/Chitosan composite[12] synthesized by Ribeiro was efficient in phosphate removal. Yuan *et al.*[13] applied the hydrotalcite-like compound composed of magnesium and iron (MF-HT) to reduce toxicities for water microorganisms in groundwater with H_2S. Layered double hydroxide (LDO), prepared by calcination of LDH at a high temperature, has more pores, a larger specific surface area, and more stable products after adsorption[14].

The chemical properties of the solid surface play a decisive role in physical and chemical processes such as solid adsorption, desorption, and ion exchange[15]. The surface complexation models (SCMs) are mainly used to study the chemical reactions occurring at the solid-liquid interface. Hydroxy proton transfer occurs in the aqueous solution, some located on the surface of the metal are called Lewis acid, and others losing protons are called Lewis base, both of which react with ligands in the solution[16,17]. Protonation and deprotonation of surface functional groups on the material make a significant contribution to the acid-base buffering capacity. At present, acid-base buffering characteristics of materials are commonly used to reflect the surface chemical properties of solid materials[18].

tetracycline hydrochloride (TCH)[19] and ofloxacin (OFX)[20] are typical representatives of tetracyclines (TCs) and quinolone antibiotics, respectively, which are two common antibiotics. Therefore, in this study, a special adsorbent for the specific antibiotic will be proposed, and the acid-base buffering properties of the materials will be investigated to study the adsorption mechanism.

EXPERIMENTAL

Materials

Urea, $Zn(NO_3)_2 \cdot 6H_2O$, $Al(NO_3)_3 \cdot 9H_2O$, HNO_3, HCl, $NaNO_3$, NaOH, Na_2CO_3, potassium hydrogen phthalate, phenolphthalein indicator, bromocresol green, methyl- red and anhydrous ethanol were purchased from Sinopharm Chemical Reagent Co. (Shanghai, China) and were analytical grade. Deionized water (around 15 MΩ/cm) was used in experiments.

Preparation

Compared with other preparation methods, the urea synthesis method achieves a larger yield and higher crystallinity[21]. 250 mL deionized water, 0.525 mol urea, 0.15 mol Zn $(NO_3)_2 \cdot 6H_2O$, and 0.075 mol Al $(NO_3)_3 \cdot 9H_2O$ were added into a 500 mL beaker, which was stirred at 105 °C in an oil bath. When the system hit 95 °C, urea decomposed into CO_3^{2-} and NH_3, and gas escaped. After 1h, the mixture gradually turned to a milky white color. The mixture was stirred for 10 h and aged at 90 °C for 20 h. After washing, filtering, and drying, Zn-Al LDH was synthesized. The LDH was put into the muffle furnace and calcined at 450 °C for 4 h to obtain LDO.

Characterizations

The crystal structures of materials were characterized with XRD (D8, Brucker, Germany). The microstructures of the materials were characterized by TEM (Talos F200S, Thermo Scientific, America) and SEM (JSM 7100F, Jeol, Japan). The specific surface areas were determined by BET (ASAP2020, Micromeritics, America). FT-IR spectrometer (Vector-22, Bruker, Germany) was used to study the adsorption mechanism.

Acid-base titration

The automated potentiometric titrator (907 Titrano, Metrohm Corporation, Switzerland) was used to determine the titration data. The material was exposed to 0.1 mol/L $NaNO_3$ solution in a water bath at 25 °C for 30 min. Then, the suspension was titrated with the standard 0.1 M HNO_3 until pH to 3.5. After stabilization for another half an hour, 0.1 M NaOH was dropwise added to the solution to bring the pH to 11. Stability of 0.005 pH/min was obtained for each titration[22]. Additionally, a control solution of 0.1 mol/L $NaNO_3$ was required[23,24].

Batch adsorption experiments

HCl and NaOH were utilized to regulate the pH of the solutions for the batch adsorption experiments. The effects of original pH (TCH: 2.5, 4.5, 6.5, 8.5, 10.5; OFX:3, 5, 7, 9, 11) on the adsorption abilities of LDH and LDO were studied, respectively. Different dosages of materials ranging from 0.02 g to 0.12 g were added to the antibiotic solutions to investigate the effects of adsorbent dosages on the adsorption effect. Samples were exposed to a range of antibiotic concentrations (TCH: 5-500 mg/L; OFX: 5-120 mg/L) for the kinetics experiments. The isotherm experiments were carried out at 293.15 K. The adsorption ability (q_e) and adsorption rate (R) are calculated as Equations (1) and (2).

$$q_e(mg/g) = \frac{C_0 - C_1}{m} \times V \quad (1)$$

$$R(\%) = \frac{C_0 - C_1}{C_0} \times 100\% \quad (2)$$

where C_0 (mg/L) and C_1 (mg/L) are the concentration of antibiotics before and after adsorption; m (g) and V (L) are the mass of adsorbent and the volume of antibiotic, respectively.

In order to study the cyclic adsorption performance, LDO after adsorption of TCH was calcined at 450 °C for 4 h for desorption. Considering the material loss during operation, TCH-LDO liquid-solid ratio was fixed at 0.25 g/L during the five-cyclic adsorption experiment[25].

RESULT AND DISCUSSION

Microstructural characterization LDH and LDO

XRD analysis

According to Figure 1A, LDH was synthesized with high crystallinity (JCPDS 48-1021). After calcination, characteristic peaks such as (003), (006), and (009) disappear and are replaced by low strength and scattered diffraction peaks, indicating that LDO lost its lamellar structure to form Zn oxide and Zn-Al composite oxides[26].

TEM analysis

The morphologies of LDH and LDO are shown in Figure 2. The obvious layered structure of LDH can be seen in Figure 2A. The crystal plane spacings of d_1 = 7.6200 nm and d_2 = 3.8100 nm correspond to (003) and (006) of LDH as in Figure 2C (JCPDS 48-1021), which also indicates that LDH was successfully prepared. Some lamellar structures are still observed in the TEM images of LDO [Figure 2B] due to "the memory effect" under the influence of ethanol during TEM measurement[27]. In Figure 2D, d_1 = 2.4759 nm and d_2 = 2.6033 nm correspond to (101) and (002) of ZnO (JCPDS 36-1451), d_3=2.442 nm corresponded to (311) of $ZnAl_2O_4$ (JCPDS 74-1138). The results are consistent with XRD characterization results.

SEM

LDH shows a distinct lamellar structure [Figure 3A], but LDO loses its lamellar structure and instead appears as a collapsed state with many micropores [Figure 3B]. The alteration of the structure of LDO may potentially enhance the adsorption capability.

BET

Based on the IUPAC classification[28], the N_2 adsorption and desorption isotherms curves of the materials are categorized as type IV, as demonstrated in Figure 4. Compared with LDH, LDO exhibits superior performance attributed to its larger surface area and pore volume, as outlined in Table 1. The result explains the SEM images and indicates that LDO has a superior adsorption capacity than LDH[29].

Batch adsorption experiments

Effects of pH and adsorbent dosage on adsorption

According to Figure 5A and B, pH has little effect on the stability of TCH and OFX but has significant effects on the adsorption abilities of the adsorbents. The performances of adsorbents for TCH and OFX reach the maximum at pH 8.5 and pH 7, respectively. Compared with the acidic condition, an alkaline environment has a more negative influence on the removal rate.

The adsorbent dosage also plays an important role in the adsorption process [Figure 3C and D]. Overall, the adsorption performance of LDO is better than that of LDH. When the dosages of LDH and LDO reach 0.1 g and 0.06 g, respectively, the removal rates of TCH and OFX tend to be steady.

Adsorption kinetics

The pseudo-first-order model and the pseudo-second-order model are applied to explore the adsorption kinetic behavior and provide a basis for the adsorption mechanism[30].

Table 1. Specific surface area (BET), capillary diameter, and volume capillaries of LDH and LDO

Materials	Surface area BET (m^2/g)	Porous diameter (nm)	Porous volume (cm^3/g)
LDH	21.11	26.10	0.14
LDO	96.15	7.77	0.19

LDH: Layered double hydroxide; LDO: layered double hydroxide.

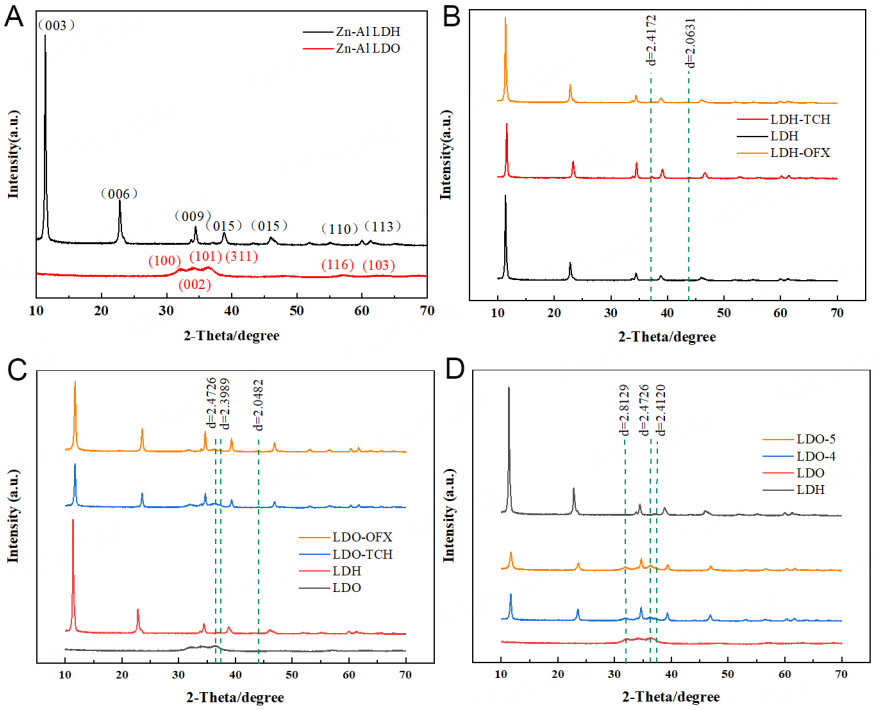

Figure 1. XRD patterns of (A) LDH, LDO; (B) before and after adsorption of LDH on TCH and OFX; (C) LDH, before and after adsorption of LDO on TCH and OFX; (D) LDH, LDO, before and after adsorption of LDO on TCH at the fourth and fifth times. LDH: Layered double hydroxide; LDO: layered double hydroxide; OFX: ofloxacin; TCH: tetracycline hydrochloride.

For the pseudo-first-order model[31]

$$\ln(q_e - q_t) = \ln q_e - K_1 t \quad (3)$$

For the pseudo-second-order model[32]

$$\frac{t}{q_t} = \frac{1}{K_2 {q_e}^2} + \frac{1}{q_e} t \quad (4)$$

where q_e and q_t are the abilities of the material adsorbing antibiotics at equilibrium and at time t (min). K_1 and K_2 separately are the constants of the two dynamics.

As shown in Figure 6 and Table 2, the correlation coefficients of the pseudo-second-order model are greater than those of the pseudo-first-order model. It demonstrates that the adsorptions are primarily chemical processes, in which the concentration of adsorbents and antibiotics jointly control the adsorption rates. In

Table 2. The kinetic parameters of antibiotics on LDH and LDO

	Pseudo-first-order model			Pseudo-second-order model		
Materials	**q_e (mg/g)**	**K_1**	**R^2**	**q_e (mg/g)**	**K_2**	**R^2**
LDH-TCH	4.86	0.013	0.886	8.028	0.125	0.982
LDH-OFX	12.12	0.025	0.868	10.018	0.100	0.990
LDO-TCH	5.67	0.055	0.927	11.132	0.090	0.989
LDO-OFX	8.10	0.019	0.970	8.774	0.114	0.983

LDH: Layered double hydroxide; LDO: layered double hydroxide; OFX: ofloxacin; TCH: tetracycline hydrochloride.

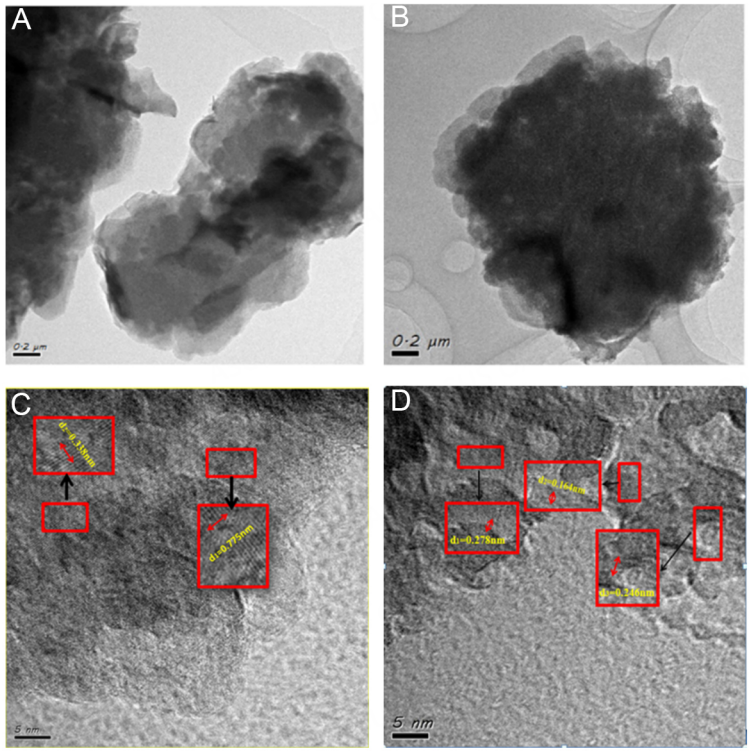

Figure 2. TEM images of (A) LDH at bar = 200 nm; (B) LDO at bar = 5 nm; (C) LDH at bar = 5 nm; (D) LDO at bar = 5 nm.

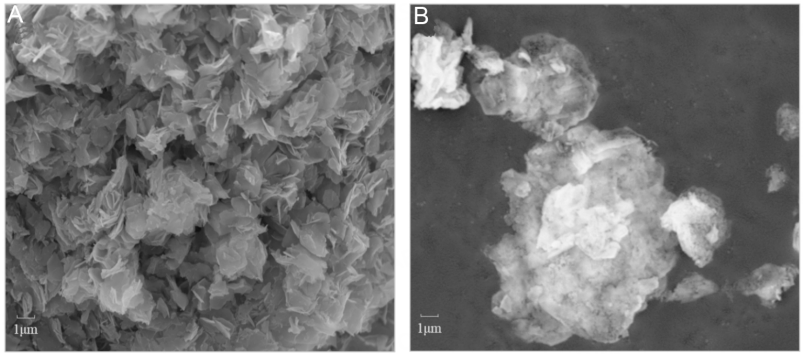

Figure 3. SEM images of (A) LDH; (B) LHO.

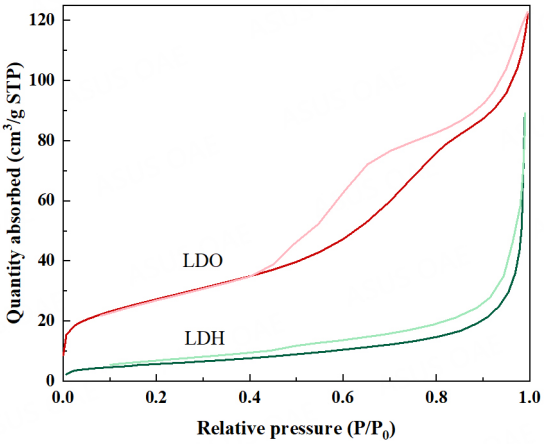

Figure 4. N_2 adsorption/desorption isotherms of LDH and LDO. LDH: Layered double hydroxide; LDO: layered double hydroxide.

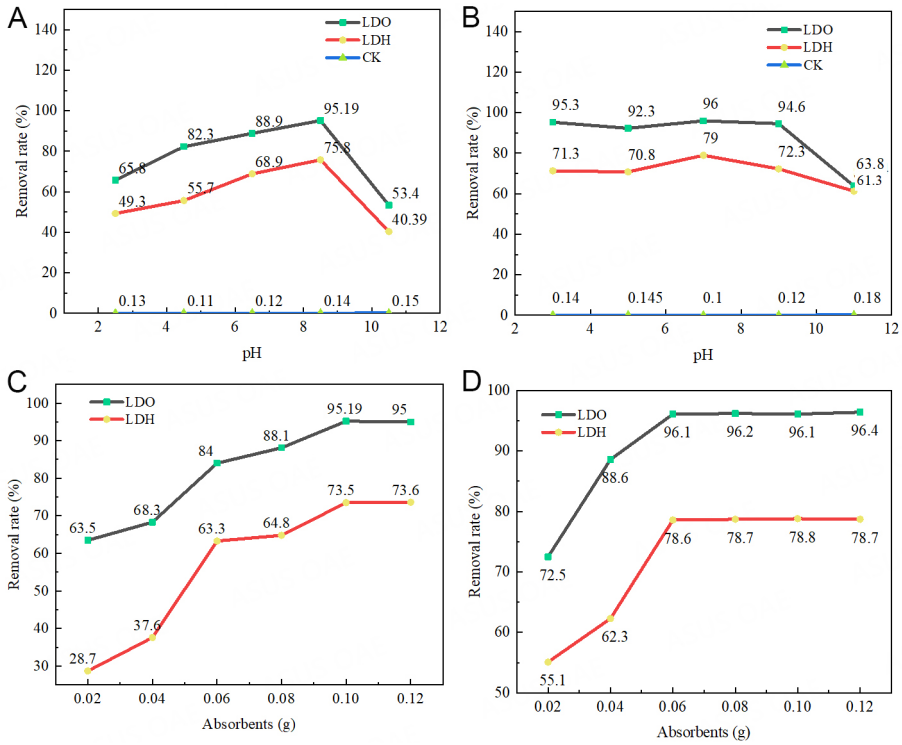

Figure 5. Effects of pH on absorption of (A) TCH (30 mg/L) and (B) OFX (20 mg/L) by LDH and LDO; effects of LDH and LDO dosage on the absorption of (C) TCH and (D) OFX. CK: Blank control group; LDH: layered double hydroxide; LDO: layered double hydroxide.

other words, the sharing and transferring of electrons between the absorbents and the antibiotics are most likely the main factors[33].

Adsorption isotherms

Adsorption isotherms are used to describe the relationship between adsorption capacity and adsorption equilibrium concentration[30]. Langmuir model and Freundlich model are commonly adsorption isotherm models, which are represented as follows.

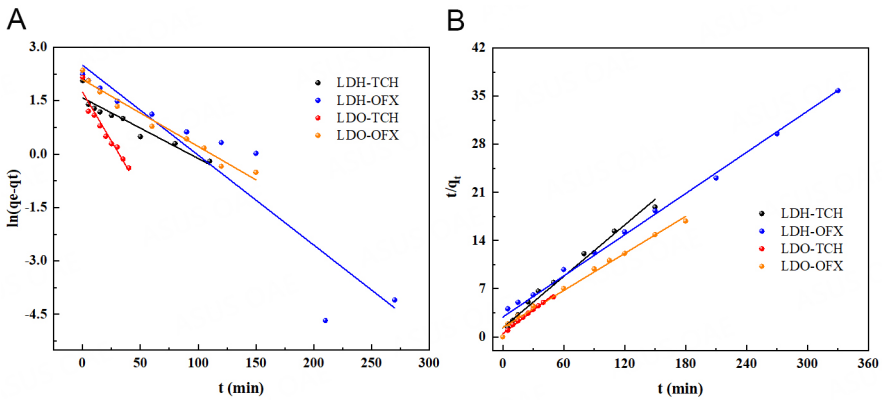

Figure 6. (A) Adsorption kinetics of LDH and LDO absorbing TCH/OFX. (A) The pseudo-first-order model; (B)the pseudo-second-order model. LDH: Layered double hydroxide; LDO: layered double hydroxide; OFX: ofloxacin; TCH: tetracycline hydrochloride.

For Langmuir model[22]:

$$\frac{C_e}{Q_e} = \frac{1}{Q_{M\times}K_L} + \frac{1}{Q_M} \times C_e \quad (5)$$

where C_e (mg/L), Q_e (mg/g), Q_M (mg/g) represent equilibrium concentration, equilibrium adsorption capacity, and maximum adsorption capacity, respectively.

Meanwhile, based on the Langmuir adsorption isotherm, the dimensionless factor R_L can be used to characterize the difficult degree of adsorption. When R_L is in the range of 0-1, it indicates that the adsorption is easy to carry out[34].

$$R_L = \frac{1}{1+K_L\times C_0} \quad (6)$$

where K_L is Langmuir constant and C_0 (mg/L) is the initial concentration.

For Freundlich model[31]:

$$Q_e = K_F \times C_e^{(1/n)} \quad (7)$$

where K_F expresses the Freundlich constant; 1/n represents adsorption intensity[35].

According to Figure 7 and Table 3, the Langmuir model is more suitable for the adsorption process than the Freundlich model. The saturated adsorption capacities of materials on TCH and OFX are 112.87, 55.04, 324.68, and 72.89 mg/g, respectively. Moreover, the dimensionless factors R_L of adsorbents adsorbing TCH and OFX calculated by Equation (6) are 0.42, 0.73, 0.259, and 0.09 mg/g, which are in the range of 0-1. It demonstrates the effective adsorption of materials and antibiotics.

Table 3. The isotherm parameters of antibiotics on LDH and LDO

	Langmuir			Freundlich		
Materials	**Q_M (mg/g)**	**K_L**	**R^2**	**1/n**	**K_F**	**R^2**
LDH-TCH	112.87	0.046	0.961	0.334	15.782	0.927
LDH-OFX	55.04	0.019	0.974	0.434	13.000	0.892
LDO-TCH	324.68	0.096	0.928	0.323	58.545	0.902
LDO-OFX	72.89	0.526	0.949	0.262	27.424	0.809

LDH: Layered double hydroxide; LDO: layered double hydroxide; OFX: ofloxacin; TCH: tetracycline hydrochloride.

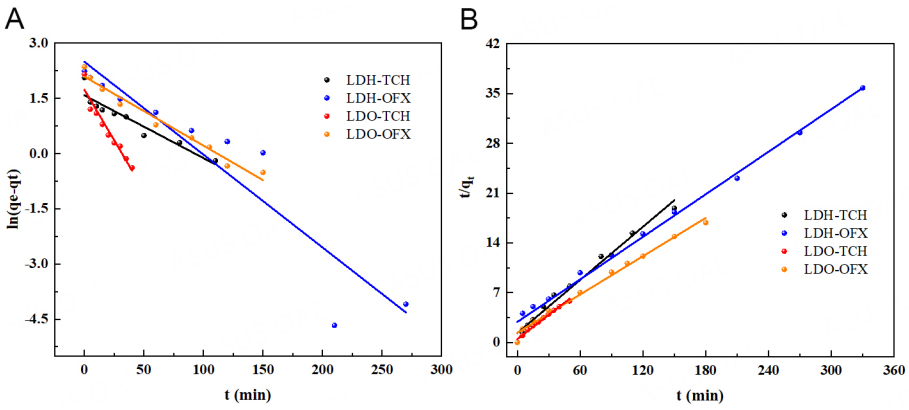

Figure 7. Adsorption isotherms of adsorbents absorbing TCH and OFX (A) Langmuir model; (B) Freundlich model. LDH: Layered double hydroxide; LDO: layered double hydroxide; OFX: ofloxacin; TCH: tetracycline hydrochloride.

Cyclic adsorption experiment

According to Figure 8, LDO has a good adsorption effect on TCH during five adsorption cycles. At the fourth adsorption, the adsorption rate begins to slow down, and the adsorption equilibrium time is extended from 50 min to 100 min. At the fifth adsorption, the removal rate decreases from 95.19% to 94.89%. Therefore, the LDO_4 finishing the fourth adsorption, and the LHO_5 finishing the fifth adsorption are characterized by XRD [Figure 1D].

LDO_4 as well as LDO_5 recover lamellar structures with the unique "memory effect"[36]. Compared with LDH, the diffraction peak intensity of LDO_4 and LDO_5 decreased significantly. Moreover, the characteristic peaks of Zn oxide and Zn-Al composite oxides appeared at 31.79° and 36.24°, which show that multiple high-temperature desorptions weaken its reconstruction performance. It explains why the fourth and fifth adsorption rates in the cyclic adsorption process have a lower adsorption rate and an extended equilibrium time. However, its obvious diffraction peaks are still observed, and the removal rate of TCH remains at 94.9%, indicating that LDO can achieve multiple cyclic adsorptions. Meanwhile, a new peak is generated at 37.29°, indicating that new substances are produced during the adsorption of TCH.

Adsorption mechanisms

FT-IR

After absorbing the antibiotics [Figure 9A], the peak at 3,447 cm^{-1} is blue-shifted, which indicates that hydrogen bonds formed between the adsorbents and the electronegative atoms of the two antibiotics. After the adsorption of TCH and OFX, the characteristic amino group peaks at 3,064 cm^{-1}, 3,060 cm^{-1}, and 2,190 cm^{-1} can be observed. It is caused by coordination complexation between the exposed aluminum as well as zinc ions at the end of the LDH and the amino groups in the structure of the two antibiotics[37]. A

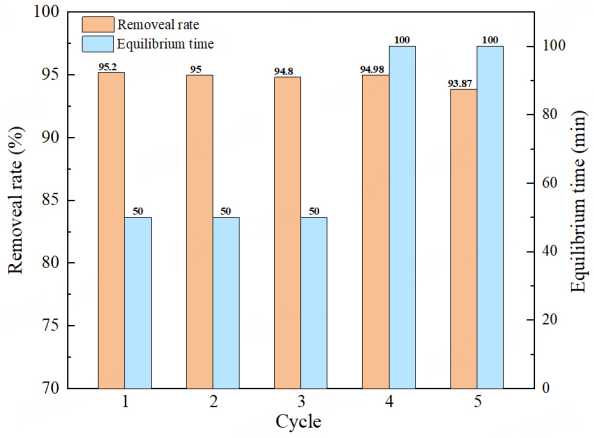

Figure 8. Cyclic adsorption experiment of TCH absorption by LDO.

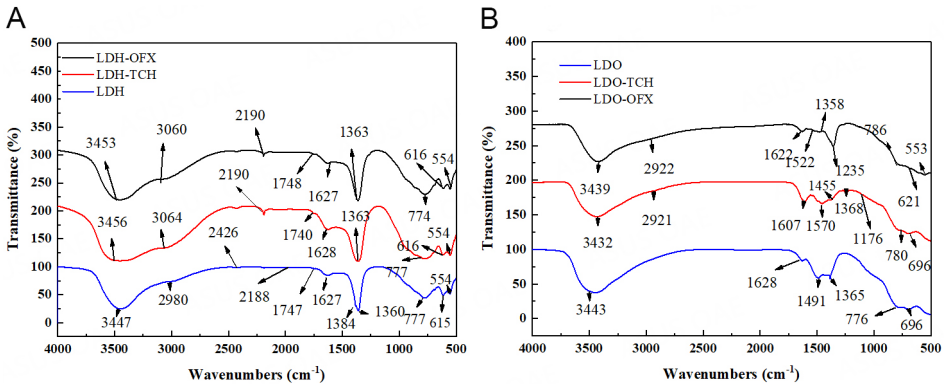

Figure 9. FT-IR spectrum comparison of (A) LDH and (B) LDO adsorbed antibiotics. LDH: Layered double hydroxide; LDO: layered double hydroxide; OFX: ofloxacin; TCH: tetracycline hydrochloride.

similar situation happens during the adsorption of LDO [Figure 9B]. In addition, after LDO adsorbing TCH, absorption peaks at 1,235 cm^{-1} and 1,176 cm^{-1} are generated in the 1,300-400 fingerprint region, which may be single bonds such as C-O, N-H, and OH- originating from TCH[38].

XRD

After the adsorption of antibiotics, the characteristic diffraction peaks intensities of LDH, particularly TCH-LDH, clearly decrease in Figure 1B. And new peaks appear, and measurements of the crystal plane spacings (d_1 = 2.4172 nm and d_2 = 2.0631 nm) confirm the complexation reaction between LDH and TCH. As shown in Figure 1C, the unique "memory effect" allows LDO to recover the layered structure during the adsorption of antibiotics. The fact that the distinctive peak of Zn/Al spinel is still present at 36.70° shows that LDO has not completely reverted. At the same time, new peaks also appear at 37.39° (d = 2.3989 nm) and 44.15° (d = 2.0482 nm), which indicate that antibiotics were absorbed by LDO due to "memory effect" and coordination reaction[39].

Acid-base buffer capacity

An automatic potentiometric titration instrument is used to perform the acid-base titration experiments on the adsorbents before and after adsorbing antibiotics, and the total acid concentration (Ht) is calculated. The H_t-pH diagrams are made by taking the H_t value as the X-axis and the pH measured at each drip point

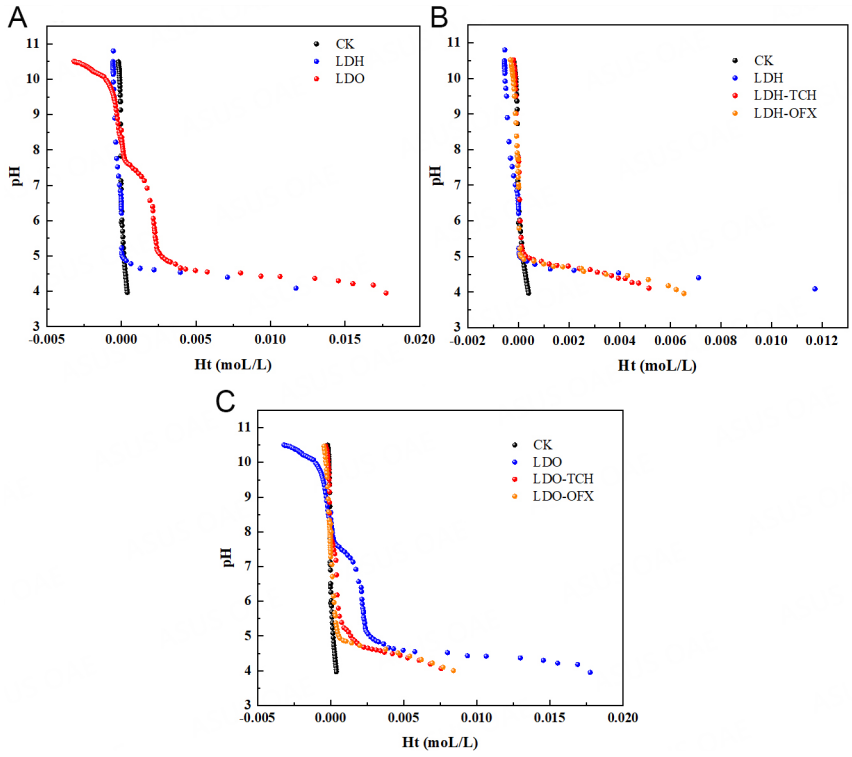

Figure 10. H_t-pH function of (A) LDH, LDO, CK; (B) CK, before and after LDH adsorbing antibiotics; (C) CK, before and after LDO adsorbing antibiotics. CK: Blank control group; LDH: layered double hydroxide; LDO: layered double hydroxide; OFX: ofloxacin; TCH: tetracycline hydrochloride.

as the Y-axis to present the acid-base buffering performance of materials[18]. H_t (mo1/L) is calculated as Equation (8)

$$Ht = \frac{V_a \times C_a - V_b \times C_b}{V_0 + V_a + V_b} \quad (8)$$

where C_a, C_b (mo1/L) separately are concentrations of HNO_3 and NaOH; V_0, V_a, and V_b (mL) are the volume of solutions before titration, the volume of consumed acid, and the volume of consumed base.

Compared with the blank control group, the suspensions of adsorbents show a stronger buffering ability to acids and bases. However, LDO performs better at acid-base buffering than LDH [Figure 10A], particularly alkaline environment, which may be related to the existence of metal oxides in LDO. The greater acid-base buffering capacity indicates more active sites on the LDO surface than LDH[18,40].

After absorbing antibiotics, the buffering abilities of LDH and LDO are significantly weakened [Figure 10B and C], indicating that their active sites on the surface are diminished. The reason for the phenomenon is that the functional groups (like Al-OH and Zn-OH) form complexes with the amino groups of antibiotics on the surface of materials, supporting the FT-IR results.

CONCLUSIONS

LDH was prepared by the urea method, and LDO was obtained by calcining LDH at 450 °C. According to the adsorption experiments of TCH and OFX, the maximum adsorption capacities of LDH and LDO for TCH are 116.28 mg/g and 322.58 mg/g at pH 8.5, and for OFX were 25.06 mg/g and 43.37 mg/g at pH 7, respectively. XRD, TEM, SEM, FI-TR, BET, and especially acid-base titration experiments indicate that the adsorption performance of LOD on the two antibiotics is better than that of LDH, which is due to more active sites on the surface, "memory effect" and bigger specific surface area. Due to the more stable quinolone ring structure of OFX, the adsorption capacity of materials to OFX is weaker than TCH. Furthermore, after five cycles of adsorption and desorption, the adsorption rate of LDO to TCH remains at 94.9%. Thus, LDO can be employed as a special adsorbent for TCH.

DECLARATIONS

Authors' contributions

Writing, formal analysis, editing: Zhang C
Review: Li Y
Validation: García-Meza JV

Availability of data and materials

Not applicable.

Ethical approval and consent to participate

Not applicable.

Consent for publication

Not applicable.

Financial support and sponsorship

This work was financially supported by Innovation Ability Improvement Project of Science and Technology smes in Shandong Province, China (Grant No.2022TSGC2501). Also, Cui Zhang would like to thank CONACyT for granting her scholarship (No. 813509) during her Ph.D. study.

Conflicts of interest

All authors declared that there are no conflicts of interest.

REFERENCES

1. Li S, Show PL, Ngo HH, Ho SH. Algae-mediated antibiotic wastewater treatment: a critical review. *Environ Sci Ecotechnol* 2022;9:100145. DOI PubMed PMC
2. García J, García-Galán MJ, Day JW, et al. A review of emerging organic contaminants (EOCs), antibiotic resistant bacteria (ARB), and antibiotic resistance genes (ARGs) in the environment: increasing removal with wetlands and reducing environmental impacts. *Bioresour technol* 2020;307:123228. DOI PubMed
3. Shin JH, Yu HJ, Park J, et al. Fluorine-containing polyimide/polysilsesquioxane carbon molecular sieve membranes and techno-economic evaluation thereof for C3H6/C3H8 separation. *J Memb Sci* 2020;598:117660. DOI
4. El-Borady OM, Fawzy M, Hosny M. Antioxidant, anticancer and enhanced photocatalytic potentials of gold nanoparticles biosynthesized by common reed leaf extract. *Appl Nanosci* ;2021:1-12. DOI
5. Abd El-Monaem EM, Eltaweil AS, Elshishini HM, et al. Sustainable adsorptive removal of antibiotic residues by chitosan composites: An insight into current developments and future recommendations. *Arab J Chem* 2022;15:103743. DOI PubMed PMC
6. Dao KC, Yang CC, Chen KF, Tsai YP. Recent trends in removal pharmaceuticals and personal care products by electrochemical

oxidation and combined systems. *Water* 2020;12:1043. DOI
7. Hu Z, Ma Y, Lu N, et al. Magnetic conjugated microporous polymer hollow spheres decorated with Fe_3O_4 nanoparticles for selective absorption and sterilization. *Environ Sci* 2022;9:1381-90. DOI
8. Mills SJ, Christy AG, Schmitt RT. The creation of neotypes for hydrotalcite. *Mineral Mag* 2016;80:1023-9. DOI
9. Tadanaga K, Furukawa Y, Hayashi A, Tatsumisago M. Direct ethanol fuel cell using hydrotalcite clay as a hydroxide ion conductive electrolyte. *Adv Mater* 2010;22:4401. DOI PubMed
10. Shirin VKA, Sankar R, Johnson AP, Gangadharappa HV, Pramod K. Advanced drug delivery applications of layered double hydroxide. *J Control Release* 2021;330:398-426. DOI PubMed
11. Yuan X, Wang Y, Wang J, Zhou C, Tang Q, Rao X. Calcined graphene/MgAl-layered double hydroxides for enhanced Cr (VI) removal. *Chem Eng J* 2013;221:204-13. DOI
12. Ribeiro NI, Pessanha OB, Pessanha MLGS, Guimaraes D. Efficient phosphate adsorption by a composite composed of $Mg_6Al_2(CO_3)(OH)_{16}.4H_2O$ LDH and Chitosan: kinetic, thermodynamic, desorption, and characterization studies. *Sep Purif Technol* 2023;307:122717. DOI
13. Yuan T, Hashimoto K, Tazaki A, et al. Potential application of a hydrotalcite-like compound for reduction of toxicity to aquatic organisms via rapid and efficient removal of hydrogen sulfide. *J Environ Manage* 2022;321:115861. DOI
14. Mandal S, Mayadevi S. Adsorption of fluoride ions by Zn-Al layered double hydroxides. *Appl Clay Sci* 2008;40:54-62. DOI
15. Hou WG, Song SE. Intrinsic surface reaction equilibrium constants of structurally charged amphoteric hydrotalcite-like compounds. *J Colloid Interface Sci* 2004;269:381-7. DOI PubMed
16. Peng L, Liu P, Feng X, et al. Kinetics of heavy metal adsorption and desorption in soil: developing a unified model based on chemical speciation. *Geochim Cosmochim Acta* 2018;224:282-300. DOI
17. Wang Y, Cheng P, Li F, et al. Variable charges of a red soil from different depths: acid-base buffer capacity and surface complexation model. *Appl Clay Sci* 2018;159:107-15. DOI
18. Yang Y, Wang Y, Peng Y, Cheng P, Li F, Liu T. Acid-base buffering characteristics of non-calcareous soils: correlation with physicochemical properties and surface complexation constants. *Geoderma* 2020;360:114005. DOI
19. Hao R, Xiao X, Zuo X, Nan J, Zhang W. Efficient adsorption and visible-light photocatalytic degradation of tetracycline hydrochloride using mesoporous BiOI microspheres. *J Hazard Mater* 2012;209:137-45. DOI PubMed
20. Deng Y, Debognies A, Zhang Q, et al. Effects of ofloxacin on the structure and function of freshwater microbial communities. *Aquat Toxicol* 2022;244:106084. DOI PubMed
21. Men Y, Fang X, Gu Q, et al. Synthesis of Ni_5Ga_3 catalyst by Hydrotalcite-like compound (HTlc) precursors for CO_2 hydrogenation to methanol. *Appl Catal B Environ* 2020;275:119067. DOI
22. Yan S, Cai Y, Li H, Song S, Xia L. Enhancement of cadmium adsorption by EPS-montmorillonite composites. *Environ Pollut* 2019;252:1509-18. DOI PubMed
23. Antelo J, Avena M, Fiol S, Lopez R, Arce F. Effects of pH and ionic strength on the adsorption of phosphate and arsenate at the goethite-water interface. *J Colloid Interface Sci* 2005;285:476-86. DOI PubMed
24. Tombácz E, Szekeres M. Colloidal behavior of aqueous montmorillonite suspensions: the specific role of pH in the presence of indifferent electrolytes. *Appl Clay Sci* 2004;27:75-94. DOI
25. Shahzad K, Najam T, Bashir MS, et al. Fabrication of Periodic Mesoporous Organo Silicate (PMOS) composites of Ag and ZnO: photo-catalytic degradation of methylene blue and methyl orange. *Inorg Chem Commun* 2021;123:108357. DOI
26. Ay AN, Zumreoglu-Karan B, Temel A. Boron removal by hydrotalcite-like, carbonate-free Mg-Al-NO73-LDH and a rationale on the mechanism. *Microporous Mesoporous Mater* 2007;98:1-5. DOI
27. Erickson KL, Bostrom TE, Frost RL. A study of structural memory effects in synthetic hydrotalcites using environmental SEM. *Mater Lett* 2005;59:226-9. DOI
28. Vu VN, Pham THT, Nguyen QD, et al. Enhanced adsorption, photocatalytic degradation efficiency of phenol red using CuZnAl hydrotalcite synthesized by co-precipitation technique. *Processes* 2022;10:1555. DOI
29. Gholami P, Dinpazhoh L, Khataee A, Orooji Y. Sonocatalytic activity of biochar-supported ZnO nanorods in degradation of gemifloxacin: synergy study, effect of parameters and phytotoxicity evaluation. *Ultrason Sonochem* 2019;55:44-56. DOI PubMed
30. Fu J, Chen Z, Wang M, et al. Adsorption of methylene blue by a high-efficiency adsorbent (polydopamine microspheres): kinetics, isotherm, thermodynamics and mechanism analysis. *Chem Eng J* 2015;259:53-61. DOI
31. Miao Y, Peng W, Wang W, et al. 3D-printed montmorillonite nanosheets based hydrogel with biocompatible polymers as excellent adsorbent for Pb(II) removal. *Sep Purif Technol* 2022;283:120176. DOI
32. Yang Y, Wang L, Zhao H, et al. Utilization of KOH-modified fly ash for elimination from aqueous solutions of potentially toxic metal ions. *Environ Res* 2023;223:115396. DOI PubMed
33. Ahmad M, Ahmad M, Usman ARA, et al. An efficient phosphorus scavenging from aqueous solution using magnesiothermally modified bio-calcite. *Environ Technol* 2018;39:1638-49. DOI PubMed
34. Ciftci TD, Coskun YI. Removal of Pb(II) from water using (Fe_3O_4/Ni/NixB) magnetic nanocomposites, carob (ceratonia siliqua) or grape seeds (vitis vinifera). *J Water Chem Technol* 2020;42:185-95. DOI
35. Long FL, Niu CG, Tang N, et al. Highly efficient removal of hexavalent chromium from aqueous solution by calcined Mg/Al-layered double hydroxides/polyaniline composites. *Chem Eng J* 2021;404:127084. DOI
36. Kwon D, Kang JY, An S, Yang I, Jung JC. Tuning the base properties of Mg-Al hydrotalcite catalysts using their memory effect. *J*

Energy Chem 2020;46:229-36. DOI

37. Kang J, Liu H, Zheng YM, Qu J, Chen JP. Systematic study of synergistic and antagonistic effects on adsorption of tetracycline and copper onto a chitosan. *J Colloid Interface Sci* 2010;344:117-25. DOI PubMed
38. Chen C, Chen D, Xie S, Quan H, Luo X, Guo L. Adsorption behaviors of organic micropollutants on zirconium metal-organic framework UiO-66: analysis of surface interactions. *ACS Appl Mater Interfaces* 2017;9:41043-54. DOI PubMed
39. Palmer SJ, Frost RL, Nguyen T. Hydrotalcites and their role in coordination of anions in Bayer liquors: anion binding in layered double hydroxides. *Coord Chem Rev* 2009;253:250-67. DOI
40. Cheng PF, Wang Y, Cheng K, Li FB, Qin HL, Liu TX. The acid base buffer capacity of red soil variable charge minerals and its surface complexation model. *ACTA Chim Sin* 2017;75:637-44. DOI